

Photocatalytic and Antimicrobial Activities of Poly(aniline-co-o-anisidine)/Zinc Oxide Nanocomposite

K. SIVAKUMAR^{1,2}, V. SENTHIL KUMAR¹, JAE-JIN SHIM³ and YUVARAJ HALDORAI^{3,*}

¹Department of Physics, Karpagam University, Coimbatore-642 120, India

²Department of Physics, Hindusthan College of Engineering and Technology, Coimbatore-641 032, India

³School of Chemical Engineering, Yeungnam University, Gyeongsan, Gyeongbuk 712-749, Republic of Korea

*Corresponding author: Fax: +82 0538104631; Tel: +82 0538103240; E-mail: yuvraj_pd@yahoo.co.in

Received: 3 September 2013;

Accepted: 9 October 2013;

Published online: 15 January 2014;

AJC-14596

The conjugated poly(aniline-co-o-anisidine)/zinc oxide [poly(Ani-co-oAs)/ZnO] nanocomposite was prepared by *in-situ* chemical oxidative polymerization of comonomers with ZnO nanoparticles and applied as a photocatalyst for the degradation of methylene blue dye. Scanning electron microscopy, transmission electron microscopy, X-ray diffraction, Fourier transform infrared spectroscopy and UV-visible spectroscopy measurements were used to characterize the resulting pure copolymer and nanocomposite. Transmission electron microscopy analysis showed that the nanoparticles with a mean diameter of 15-25 nm were dispersed in the copolymer matrix. Thermogravimetric analysis indicated that the nanocomposite had a higher decomposition temperature than the pure copolymer. The conductivity measurements showed the resulting nanocomposite possessed higher conductivity as compared to the pure copolymer. The photocatalytic activity results indicated the degradation of methylene blue dye by 97 % over the surface of nanocomposite catalyst under UV-irradiation for 3 h. The nanocomposite exhibited good antimicrobial activity against the microbial species and the clear zone diameter of the microbial inhibition is correlated to the antimicrobial activity of nanocomposite.

Keywords: Polyaniline, Poly(o-anisidine), Metal oxide, Nanocomposite, Photocatalyst, Antimicrobial agent, Methylene blue.

INTRODUCTION

Recently, there has been increasing interest to the development of organic/inorganic hybrid materials on nanometer scale has grown due to their wide range of potential applications^{1,2}. Nanocomposite materials composed of conducting polymers and metal oxides have opened more fields of applications such as drug delivery, conductive paints, rechargeable batteries, toners in photocopying, smart windows, *etc.*³. Inorganic fillers at nanoscale exhibit quite different electronic and optical properties from those of their bulk state. It is expected to obtain a new composite material that has synergetic or complementary behaviors between the polymer and inorganic material. Conducting polymers provide tremendous scope for tuning of their electrical conductivity from semiconducting to metallic region by way of doping⁴ and are organic electro-chromic materials with chemically active surface. Among the conducting polymers, polyaniline is one of the promising polymers due to high conductivity, simple synthesis procedure, good environmental stability and reversible acid base chemistry in aqueous solution and large variety applications^{5,6}.

Nanosized inorganic semiconductor materials have attracted considerable interest in recent years. Among the inorganic semiconductors, ZnO is a wide band gap semicon-

ductor (3.37 eV) with an exciton binding energy of 60 meV, which permits laser emission at room temperature. This large band gap is suitable for the use of ZnO to collect high-energy photons (UV light). These attractive physical properties made ZnO a potential candidate for the optoelectronic applications⁷. In addition, nanoscale ZnO has been found to exhibit marked antimicrobial activity and the use of metal oxide as an antimicrobial agent has the advantages of improved safety and stability as compared to organic antimicrobial agents⁸.

There are several studies reporting the synthesis, morphology, optical, electrical and photocatalytic properties of ZnO/polyaniline nanocomposites⁹⁻¹⁶. However, most conducting polymers suffer from some limitations. For example, polyaniline with alkyl substituents presents limitations that are imposed on the conductivity of the produced polymer despite its solubility being improved when compared with polyaniline. Efforts have been made towards the design of new conducting materials. In this way, the conductivity of polyanilines and the solubility of substituted polyanilines can be achieved by copolymerization¹⁷. Copolymerization allows chemical modification as well as the introduction of specific functional groups to side substituents to control the physicochemical properties of materials¹⁸. As one of the influential derivatives of polyaniline, poly(o-anisidine) (PoAs) has been widely synthesized by

chemical oxidative polymerization¹⁹. Among the conducting copolymers, poly(Ani-*co-o*As) has attracted much attention due to its solubility and film forming property¹⁹. Recently, nanocomposites of conducting copolymers with inorganic fillers were prepared for various applications²⁰⁻²⁶. Even though, there are few reports on the synthesis of nanocomposites composed of polyaniline and its derivatives with inorganic fillers, there is no report on the synthesis of poly(Ani-*co-o*As)/ZnO nanocomposite.

In this study, we describe the synthesis, photocatalytic and antimicrobial activities of poly(Ani-*co-o*As)/ZnO nanocomposite. The ZnO nanoparticles used in this study to produce nanocomposite are synthesized by thermal decomposition method. The nanocomposite is characterized by SEM, TEM, XRD, FTIR, UV-visible and TGA. In addition, the conductivity of nanocomposite is also measured.

EXPERIMENTAL

Aniline, *o*-anisidine, zinc(II) nitrate hexahydrate, benzoic acid and hydrazine monohydrate were purchased from Aldrich. Ammonium persulfate and all other organic reagents were of analytical grade and used without further purification.

Synthesis of ZnO nanoparticles: ZnO nanoparticles were synthesized according to the procedure given in the literature²². In a typical experiment, 0.01 mole of zinc(II) nitrate hexahydrate and 0.02 mol hydrazinium benzoate were mixed *in situ* with constant stirring. The resulting mixture was concentrated to one third of its volume. The mixture was cooled, filtered, washed with alcohol and dried. Thus the precursor complex, zinc benzoate dihydrazinate formed was taken in a clean silica crucible and heated to 200 °C (for 2 h) during which the complex decomposed completely to produce the ZnO nanoparticles.

Synthesis of poly(Ani-*co-o*As)/ZnO copolymer: Monomers, aniline (0.93 g, 0.1 M) and *o*-anisidine (1.23 g, 0.1 M) were dissolved in 100 mL of a 0.1 M hydrochloric acid (HCl). Then, ammonium persulfate (2.28 g, 0.1 M) dissolved in 100 mL of a 0.1 M HCl solution was added dropwise and stirred continuously for 24 h to complete the reaction. The resulting product was thoroughly washed with deionized water until the solution turned colorless. The product was dried in a vacuum oven at 50 °C for 24 h.

Synthesis of poly(Ani-*co-o*As) nanocomposite: In a typical experiment, monomers, aniline (0.93 g, 0.1 M) and *o*-anisidine (1.23 g, 0.1 M) were dissolved in 100 mL of a 0.1 M HCl. ZnO nanoparticles (5 and 10 % w/w based on the comonomer content) were then dispersed in the solution by intense stirring for 0.5 h. Finally, ammonium persulfate (2.28 g, 0.1M) dissolved in 100 mL of a 0.1 M HCl solution was added dropwise and stirred continuously for 24 h to complete the reaction. The resulting product was thoroughly washed with deionized water until the solution turned colorless. The product was dried in a vacuum oven at 50 °C for 24 h. The nanocomposite containing 10 % ZnO was chosen for this study because of its significantly higher conductivity than the 5 % nanocomposite.

Photocatalytic activity: Methylene blue dye was used as a probe molecule to evaluate the photocatalytic activity of nanocomposite. The photocatalytic reaction was conducted at room temperature under UV light at a wavelength of 365 nm.

The 10 ppm methylene blue solution was prepared in 100 mL of deionized water. Then, 0.5 g of the nanocomposite powder was added to the methylene blue solution with uniform stirring. Prior to irradiation, the suspension was magnetically stirred in the dark for 0.5 h to establish the adsorption/desorption equilibrium of methylene blue. A 10 mL of the sample was withdrawn for every 1 h. Before analysis, the suspension was centrifuged to remove any suspended solid catalyst particles. The residual concentration of dye was measured using a Shimadzu 2450 UV-visible spectrophotometer.

Antimicrobial activity: The antimicrobial activity of poly(Ani-*co-o*As)/ZnO nanocomposite was examined by a paper disc method. The bacterial species *Staphylococcus aureus*, *Pseudomonas aeruginosa*, *Escherichia coli* and the fungal species *Aspergillus niger*, *Aspergillus flavus* used in this study were the sequenced strains. All disks and materials were sterilized in an autoclave before the experiment and all antibacterial tests were carried out in triplicate. Overnight cultures were re-grown to an optical density at 600 nm of 1.0 and about 10⁴ cells per plate was spread on Muller Hinton agar for antibacterial studies and Sabourands dextrose agar for antifungal studies. 20 µL stock solutions of nanocomposite (50 µg mL⁻¹) in ethanol were dispensed on sterile paper discs (Whatman No.1) of 6 mm diameter. Plates were incubated at 37 °C for overnight and the antimicrobial activity of nanocomposite was evaluated by measuring the zones around the discs. Ethanol was used as a control sample.

Characterization: UV-visible spectrum of the diluted nanocomposite dispersion in the 200-800 nm range was obtained using a Shimadzu 2450 spectrophotometer. Microscopic images of nanocomposites were obtained by a JEOL 6390 scanning electron microscope (SEM). The samples were gold-coated prior to examination. TEM images were obtained on a transmission electron microscope (JEOL-2010) operated with an accelerating voltage of 200 kV. The sample was prepared as follows: a small amount of the nanocomposite sample was dispersed in alcohol under ultrasonication for 5 min. One drop of the dilute suspension was deposited on a copper grid coated with a carbon membrane. FT-IR characterizations were performed using a Shimadzu spectrometer. Room temperature conductivities of the pressed pellets were measured using a standard four-point probe method (Keithley model 196 system digital multimeter). Thermogravimetric analysis (TGA) was performed on a TG/DTA EXSTAR 6000 series from room temperature to 700 °C at a heating rate of 10 °C/min under nitrogen atmosphere. The phase and crystallinity were characterized using a Shimadzu 6000 X-ray diffractometer with CuK_α radiation in the 2θ range of 10-80°.

RESULTS AND DISCUSSION

The synthesis and characterization of ZnO nanoparticles (15-25 nm) by thermal decomposition method were described in our previous work²². In this article, we synthesized the poly(Ani-*co-o*As)/ZnO nanocomposite by chemical oxidative polymerization using ammonium persulfate as an oxidant and HCl as a dopant. The nanocomposite was characterized by FT-IR, SEM, TEM, UV-visible, TGA and XRD. In addition, conductivity, photocatalytic property and antimicrobial activity were discussed.

Typical FT-IR spectra of the pure copolymer and nanocomposite with 10 % ZnO are shown in Fig. 1. It is clear that the copolymer and composite showed similar spectra. The band centered at 3283 cm^{-1} was attributed to the characteristic N-H stretching vibration of a secondary amine²⁷. The bands at 1690 and 1500 cm^{-1} were assigned to C=C stretching vibrations of quinoid and benzenoid rings, respectively²⁸. The band at 1298 cm^{-1} was attributed to the C-N stretching vibration in the quinoid imine units. The band at 1198 cm^{-1} was the characteristic peak of polyaniline conductivity and is a measure of the degree of the delocalization of electrons²⁹. The band corresponding to out of plane bending vibration of C-H bond of *p*-disubstituted rings appeared at 805 cm^{-1} . The appearance of these IR bands varified the formation of copolymer. In the nanocomposite, we observed the respective vibrational bands of the both copolymer and ZnO (The Zn-O band appeared at 452 cm^{-1}). However, the incorporation of ZnO led to the obvious shift of some FT-IR bands in the spectrum of nanocomposite when compared to the pure copolymer. The shift may be described due to the formation of hydrogen bonding on the surface of ZnO nanoparticles and -NH-group of copolymer.

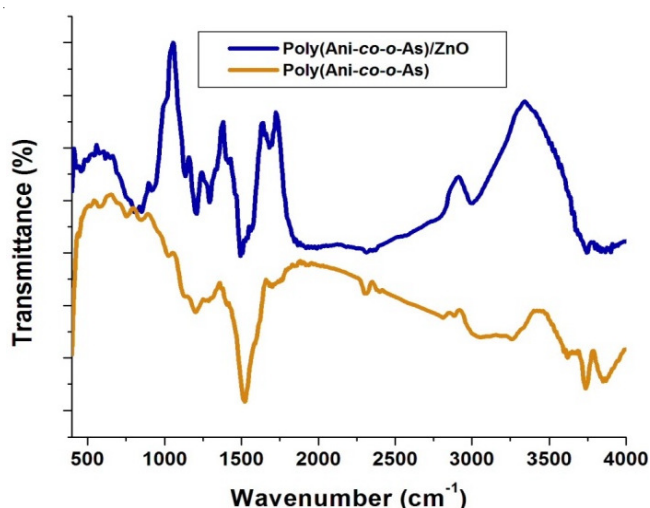


Fig. 1. FT-IR spectra of the pure copolymer and poly(Ani-co-o-As)/ZnO nanocomposite

Fig. 2 shows the SEM images of pure copolymer and nanocomposite. It was observed that the as synthesized copolymer (Fig. 2a) showed a typical morphology, whereas the nanocomposite (Fig. 2b) showed a growth of a chain pattern of copolymer and the ZnO nanoparticles were present between the junctions of the copolymer chain network. Fig. 2b showed that the nanoparticles are almost uniform, global and slightly agglomerated. The phase contrast of the nanocomposite appears to be less pronounced owing to the engulfment of ZnO nanoparticles by the copolymer. The micrograph of nanocomposite revealed a two-phase system where the bright phase corresponds to the existence of ZnO, while dark phase constitutes the copolymer.

Fig. 3 depicts the TEM picture of poly(Ani-co-o-As)/ZnO nanocomposite. The composite particles are almost spherical in shape, in which ZnO nanoparticles (average diameter of about 15-20 nm) were homogeneously dispersed in the copolymer

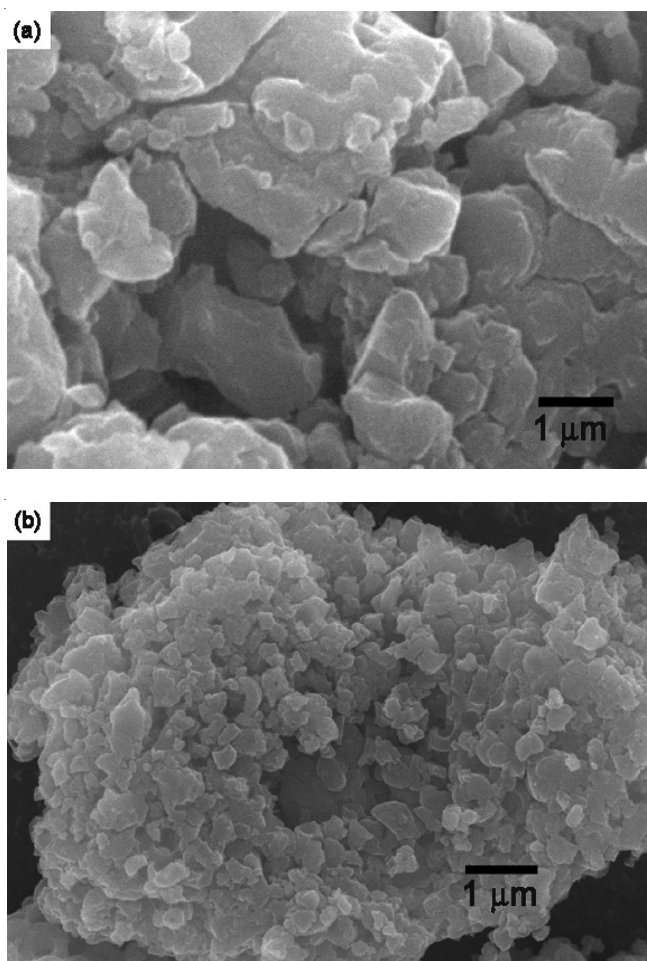


Fig. 2. SEM images of the (a) pure copolymer and (b) poly(Ani-co-o-As)/ZnO nanocomposite

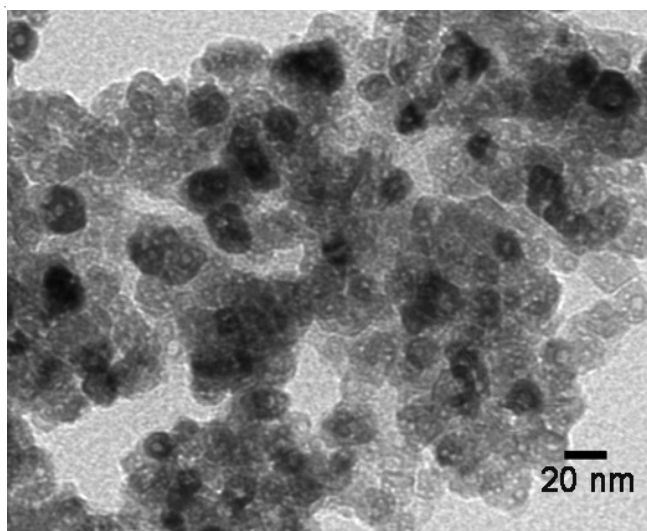


Fig. 3. TEM image of the poly(Ani-co-o-As)/ZnO nanocomposite

matrix. After composite formation, ZnO nanoparticles (dark shaded) were found to be entrapped in the copolymer chain (light shaded). Therefore, the nanoparticles were not simply mixed up or blended with the copolymer; they were rather bound by the copolymer chain. This may be ascribed that the interaction of ZnO and copolymer was followed by the formation of H-bonding between the proton on N-H and the oxygen atom

on ZnO surface. Generally blending of ZnO nanoparticles with copolymer may lead to separation in discrete phases. Because of the smaller dimensions of the ZnO nanoparticles, it is possible that several ZnO nanoparticles are coalesced to form large ZnO particles.

Thermal stability of nanocomposite with 10 % ZnO was analyzed by TGA in nitrogen and the result was compared with the pure copolymer as shown in Fig. 4. All the samples followed a similar decomposition trend with exhibiting a gradual weight loss. The initial weight loss step in TGA curve of the copolymer between 50-120 °C corresponds to the loss of water and adsorbed HCl. From 150 °C, a continuous degradation occurs until a major decomposition obtained in the region between 300-450 °C. However, it was found that the thermal stability of nanocomposite was higher than the pure copolymer which was obviously related to the existence of thermally stable ZnO. The residual mass left at 700 °C was found to be 2 and 15 % for the copolymer and nanocomposite, respectively.

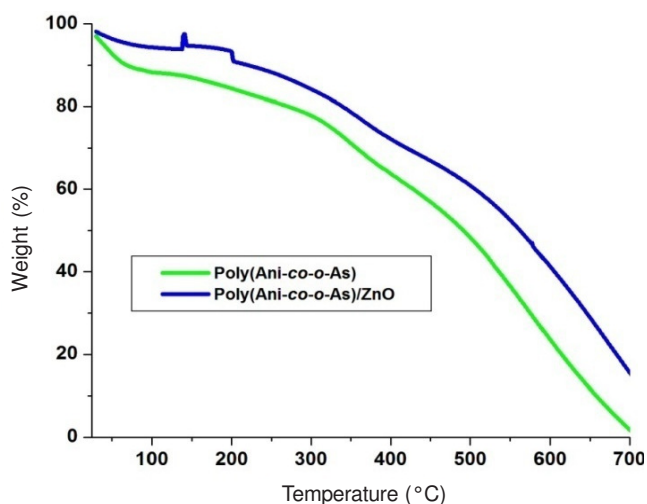


Fig. 4. TGA curves of the pure copolymer and poly(Ani-*co-o*-As)/ZnO nanocomposite in nitrogen

UV-visible spectra of the pure copolymer and nanocomposite are shown in Fig. 5. It is clear that the spectra of copolymer and composite similarly consisted of two major absorption bands. The first absorption band in the region of around 310 nm is characteristic of π - π^* transition of the benzenoid ring of the copolymer. This is related to the extent of conjugation between the phenyl rings along the copolymer chain³⁰. The second characteristic band at around 590 nm is assigned to the localized polarons³¹. In the nanocomposite, the exciton absorption at around 335 nm can be assigned to the intrinsic band-gap absorption of ZnO. However, in the nanocomposite, the copolymer absorption bands were slightly shifted. This might be due to the interaction between the nanoparticles and copolymer chains.

The XRD patterns of pure copolymer and nanocomposite are shown in Fig. 6. In the pattern, the peak centered at 25.1° was assigned to the periodicity perpendicular to the copolymer chain³². In addition, we observed several other sharp peaks at 44.1, 64.5 and 77.6° suggest that the copolymer is semi-crystalline. The XRD pattern of nanocomposite showed the peaks

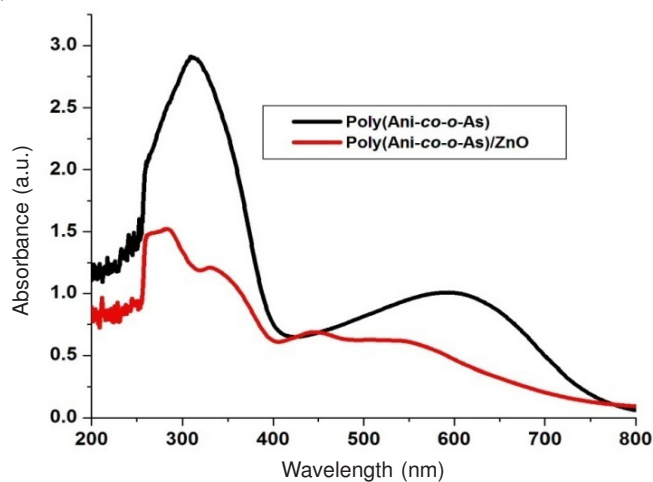


Fig. 5. UV-visible spectra of the pure copolymer and poly(Ani-*co-o*-As)/ZnO nanocomposite

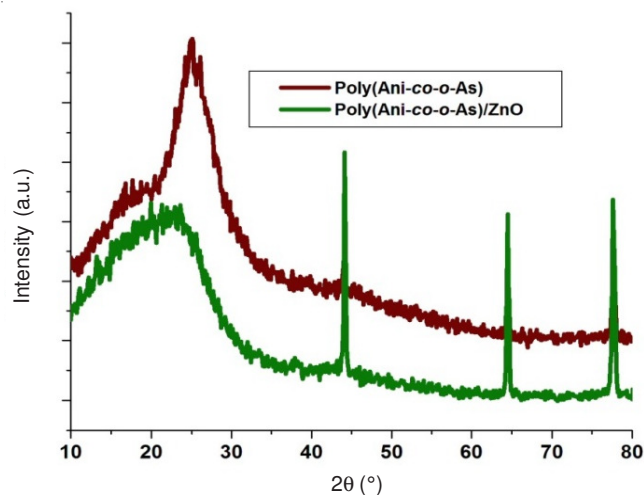


Fig. 6. XRD patterns of the pure copolymer and poly(Ani-*co-o*-As)/ZnO nanocomposite

of corresponding copolymer and no additional characteristic peaks of ZnO nanoparticles were observed. This result may be attributed to the low ZnO/comonomer ratio and the degree of polymerization.

The room temperature conductivity of the copolymer and composites varies over a range from 2.07×10^{-4} S/cm to 7.64×10^{-3} S/cm. The conductivity of copolymer, poly(Ani-*co-o*-As) was found to be 2.07×10^{-4} S/cm. The conductivity of nanocomposite was increased by one order of magnitude (1.50×10^{-3} S/cm) by the introduction of 5 % ZnO. With further increasing the ZnO content in the nanocomposite to 10 %, the conductivity increased up to the value of 7.64×10^{-3} S/cm. The concentration of ZnO nanoparticles significantly affects the conductivity of resulting nanocomposite. The conductivity of conjugated polymer based composite nanostructures is mainly dependent on the doping level of polymer, compactness of the sample, crystallinity, size, morphology of the nanocomposite and preparation method, *etc.* The reason for improvement in conductivity was attributed to the interaction between ZnO and the copolymer chain which effectively improves the degree of electron delocalization between the two components¹³.

UV-visible spectra of methylene blue solution with the photocatalyst, poly(Ani-co-oAs)/ZnO nanocomposite were recorded before and after varying durations of UV-irradiation (Fig. 7a). The intensity of the peak at 663 nm corresponds to the methylene blue, decreased with increasing UV-exposure, indicating that the methylene blue degraded under UV-irradiation. Approximately 97 % of the methylene blue was degraded by the nanocomposite within 3 h (Fig. 7b). The enhanced photocatalytic activity was due to the presence of ZnO nanoparticles in the composite.

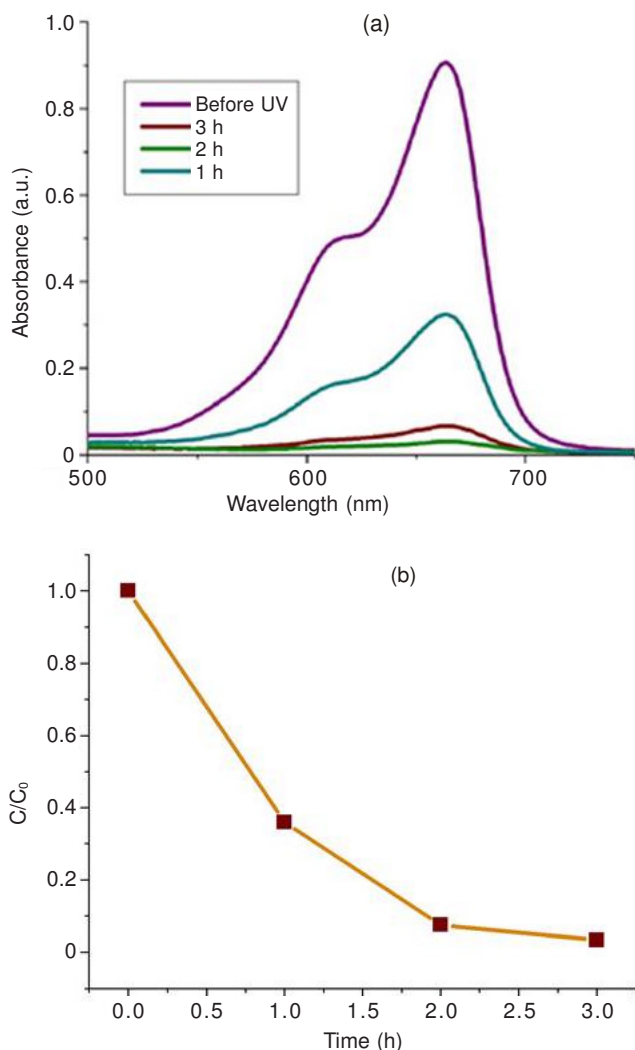


Fig. 7. (a) UV-visible spectra of methylene blue solution in the presence of poly(Ani-co-oAs)/ZnO nanocomposite at different UV-irradiation time and (b) photodegradation of methylene blue

The photo-stability of nanocomposite was investigated based on its photocatalytic performance under UV-light irradiation with three times of cycling, as shown in Fig. 8. It can be seen that the recycled use of composite for three times does not conspicuously affect its photocatalytic activity. Apparently, the composite was stable under the studied conditions and the photocorrosion effect of ZnO was effectively inhibited by conducting copolymer.

In general, the kinetics of photocatalytic degradation of organic pollutant on the semiconducting oxide has been established and can be described well by the apparent first-

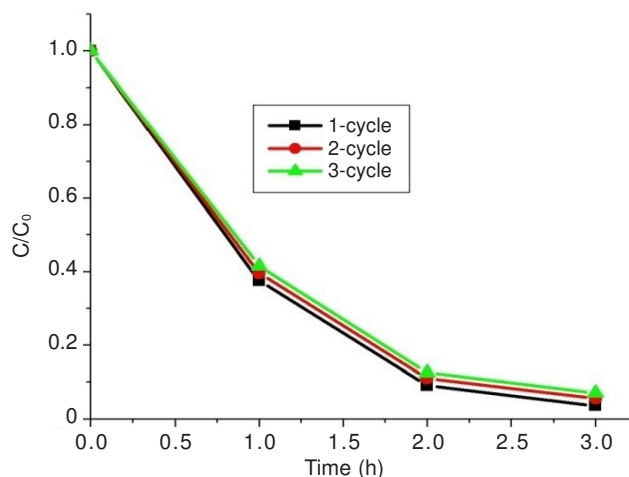


Fig. 8. Photo-stability of nanocomposite after three times of recycling uses

order reaction $\ln(C_0/C) = k_{app} \times t$, where k_{app} is the apparent rate constant, C_0 is the initial concentration of the dye and C is the concentration of dye at time t . Fig. 9 shows the apparent rate constant of methylene blue in the presence of photocatalyst under UV-light irradiation. The linear correlation of the plot of $\ln(C_0/C)$ versus time suggested a pseudo first-order reaction for the dye. The apparent rate constant was determined as 0.017 min^{-1} .

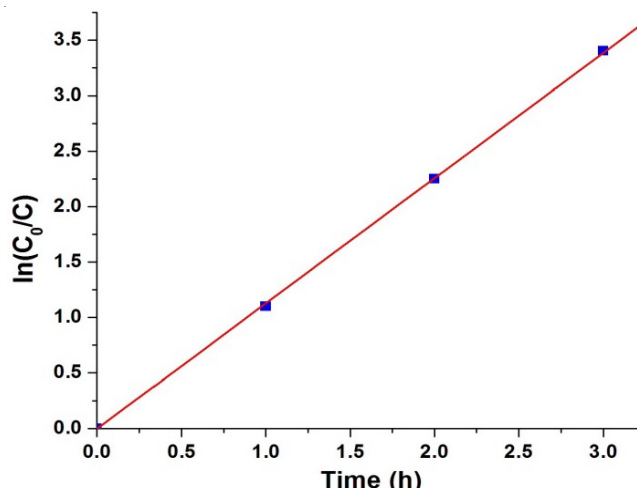


Fig. 9. Apparent rate constant of methylene blue in the presence of the photocatalyst under UV light irradiation

In this study, an investigation of antimicrobial activity of poly(Ani-co-oAs)/ZnO nanocomposite was carried out qualitatively against the bacterial species *S. aureus*, *P. aeruginosa*, *E. coli* and the fungal species *A. niger*, *A. flavus* using a paper disc method. A paper disc was wetted with the sample solution (20 μL). The agar in Petri dish was inoculated with microbial species and then the paper disc was placed on the Petri dish and pressed gently. The samples were incubated at 37°C for overnight. The presence of a clear zone that formed around the disc on the plate medium was recorded as an indication of inhibition against the microbial species (Fig. 10). The clear zone on the surface of the test specimen was observed by the naked eye and compared to the ethanol as a control sample. The clear zone diameter of the microbial inhibition correlated to the antimicrobial activity of nanocomposite and is given in

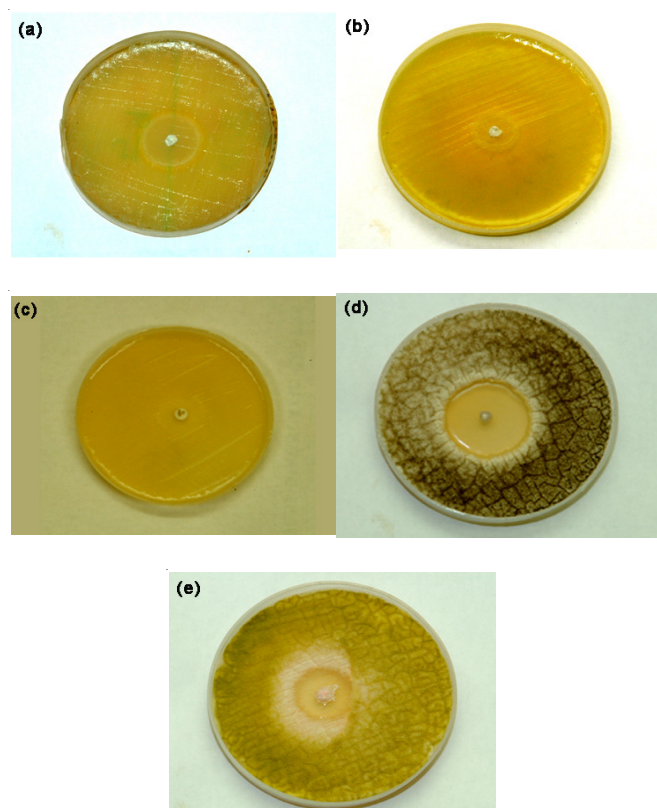


Fig. 10. Pictures of the microbial inhibition zone test of the poly(Ani-co-oAs)/ZnO nanocomposite against (a) *S. aureus*, (b) *P. aeruginosa*, (c) *E. coli*, (d) *A. niger* and (e) *A. flavus*

Table-1. The nanocomposite exhibited stronger antibacterial activities against *E. coli* than against *S. aureus* and *P. aeruginosa*. The lower efficacy against *S. aureus* and *P. aeruginosa* may have been derived from the difference in membrane structure. Gram-positive and Gram-negative bacteria have different membrane structures, the most distinctive of which lies in the thickness of the peptidoglycan layer. The peptidoglycan layer of the cell walls of Gram-positive bacteria (about 20-80 nm) is usually thicker than that of Gram negative bacteria (about 7-8 nm)³³. The thicker cell wall structures of *S. aureus* and *P. aeruginosa* may hinder the passage of the toxic agent from solution to the membrane to a greater extent. Hence, the difference in antibacterial activity is tentatively attributed to the differences in cell wall structures, *i.e.*, the permeability and structural integrity of bacteria membranes^{34,35}. The nanocomposite also showed better antifungal activity. They exhibited stronger antifungal activity against *A. flavus* than *A. niger*. Although the real mechanism of the antifungal activity of the ZnO is still uncertain, one possible explanation of the antifungal effect of ZnO is based on the abrasive surface texture of ZnO. Nano ZnO has been found to be abrasive due to surface defects. The penetration of the cell envelope and disorganization of the fungal membrane upon contact with the ZnO is also responsible for the inhibition of fungal growth.

Conclusion

We successfully synthesized poly(Ani-co-oAs)/ZnO nanocomposite by *in-situ* chemical oxidative polymerization in the presence of HCl as the dopant. TEM results confirmed that all the ZnO nanoparticles (with a mean diameter of 15-20

TABLE-1
ANTIMICROBIAL ACTIVITY OF THE
POLY(Ani-co-oAs)/ZnO NANOCOMPOSITE

Species	Clear zone diameter (mm)
<i>S. aureus</i>	20 ± 0.4
<i>P. aeruginosa</i>	17 ± 0.3
<i>E. coli</i>	24 ± 0.6
<i>A. niger</i>	13 ± 0.2
<i>A. flavus</i>	21 ± 0.5

nm) were encapsulated by the copolymer. XRD patterns showed that the nanocomposite was semi-crystalline in nature, similar to the pure copolymer. The nanocomposite showed higher thermal stability than the pure copolymer due the existence of thermally stable ZnO. The structural and the absorption studies demonstrated the shifting and changes in the relative intensity of the peaks which confirmed the effective interaction between the copolymer and ZnO through hydrogen bonding between the imine (-NH) of copolymer and the hydroxyl (-OH) group of ZnO nanoparticles. The room-temperature conductivity of nanocomposite was increased by one order of magnitude with the addition of 10 % ZnO. The nanocomposite catalyst exhibited a high photocatalytic activity of 97 % for the photodegradation of the methylene blue under UV-light irradiation for 3 h. The results showed that the repeated use of recycled composite (three times) did not affect its photocatalytic activity significantly. The nanocomposite exhibited good antimicrobial activity against *S. aureus*, *P. aeruginosa*, *E. coli*, *A. niger* and *A. flavus*. The antimicrobial activity depends on the permeability and penetration rate against the microbial cell wall.

REFERENCES

- B.W. J.E. Beek, L.H. Slooff, M.N. Wienk, J.M. Kroon and R.A.J. Janssen, *Adv. Funct. Mater.*, **15**, 1703 (2005).
- C.L. Sui, C.L. Shao and Y.C. Liu, *Appl. Phys. Lett.*, **87**, 113115 (2005).
- R. Gangopadhyay and A. De, *Chem. Mater.*, **12**, 608 (2000).
- B. Wessling, in ed: T.A. Skotheim, R.L. Elsenbaumer and J.R. Reynolds, *Handbook of Conducting Polymers*, Marcel Dekker, New York, pp. 467-530 (1998).
- G. Gustafsson, Y. Cao, G.M. Treacy, F. Klavetter, N. Colaneri and A.J. Heeger, *Nature*, **357**, 477 (1992).
- M.J. Sailor, E.J. Ginsburg, C.B. Gorman, A. Kumar, R.K. Grubbs and N.S. Lewis, *Science*, **249**, 1146 (1990).
- Z. Wang and H.L. Li, *Appl. Phys., A Mater. Sci. Process.*, **74**, 201 (2002).
- A. Lipovsky, Y. Nitzan, A. Gedanken and R. Lubart, *Nanotechnology*, **22**, 105101 (2011).
- S. Ameen, M.S. Akhtar, Y.S. Kim, O.-B. Yang and H.-S. Shin, *Colloid Polym. Sci.*, **289**, 415 (2011).
- M. Chang, X.L. Cao, H. Zeng and L. Zhang, *Chem. Phys. Lett.*, **446**, 370 (2007).
- Y. He, *Powder Technol.*, **147**, 59 (2004).
- Y. He, *Appl. Surf. Sci.*, **249**, 1 (2005).
- A.A. Khan and M. Khalid, *J. App. Polym. Sci.*, **117**, 1601 (2010).
- G.K. Paul, A. Bhaumik, A.S. Patra and S.K. Bera, *Mater. Chem. Phys.*, **106**, 360 (2007).
- S. Sharma, M. Suryanarayana, A. Nigam, A. Chauhan and L. Tomar, *Catal. Commun.*, **10**, 905 (2009).
- B.K. Sharma, A.K. Gupta, N. Khare, S.K. Dhawan and H.C. Gupta, *Synth. Met.*, **159**, 391 (2009).
- A.L. Schemid, L.M. Lira and S.I. Córdoba de Torresi, *Electrochim. Acta*, **47**, 2005 (2002).
- H. Kaczmarek and W. Czerwinski, *Photochem. Photobiol. A*, **146**, 207 (2002).
- A.D.J. Borkar, *Chem. Pharm. Res.*, **4**, 2081 (2012).

20. Y. Zhang X. Liu and Q. Li, *J. Appl. Polym. Sci.*, **128**, 1625 (2013).
21. R. Tang, Q. Li, H. Cui, Y. Zhang and J. Zhai, *Polym. Adv. Technol.*, **22**, 2231 (2011).
22. K. Sivakumar, V. Senthilkumar and Y. Haldorai, *Compos. Interfaces*, **19**, 397 (2012).
23. D.D. Borole, U.R. Kapadi, P.P. Mahulikar and D.G. Hundiwale, *Polym. Plast. Technol.*, **47**, 643 (2008).
24. Y. Haldorai, W.S. Lyoo and J.-J. Shim, *Colloid Polym. Sci.*, **287**, 1273 (2009).
25. Y. Haldorai, P.Q. Long, S.K. Noh, W.S. Lyoo and J.-J. Shim, *Polym. Adv. Technol.*, **22**, 781 (2011).
26. Y. Haldorai, V.H. Nguyen, Q.L. Pham and J.-J. Shim, *Compos. Interfaces*, **18**, 259 (2011).
27. X.G. Li, H.Y. Wang and M.R. Huang, *Macromolecules*, **40**, 1489 (2007).
28. H. Xia and Q. Wang, *J. Appl. Polym. Sci.*, **87**, 1811 (2003).
29. E.M. Scherr, A.G. MacDiarmid, S.K. Manohar, J.G. Masters, Y. Sun, X. Tang, M.A. Druy, P.J. Glatkowski, V.B. Cajipe, J.E. Fischer, K.R. Cromack, M.E. Jozefowicz, J.M. Ginder, R.P. McCall and A.J. Epstein, *Synth. Met.*, **41**, 735 (1991).
30. M. Atobe, A. Chowdhury, T. Fuchigami and T. Nonaka, *Ultrason. Sonochem.*, **10**, 77 (2003).
31. S.-J. Su and N. Kuramoto, *Synth. Met.*, **114**, 147 (2000).
32. J.P. Pouget, C.H. Hsu, A.G. MacDiarmid and A.J. Epstein, *Synth. Met.*, **69**, 119 (1995).
33. J.S. Kim, E. Kuk, K.N. Yu, J.H. Kim, S.J. Park, H.J. Lee, S.H. Kim, Y.R. Park, Y.H. Park, C.Y. Hwang, Y.K. Kim, Y.S. Lee, D.H. Jeong and M.-H. Cho, *Nanomedicine*, **3**, 95 (2007).
34. R. Brayner, R. Ferrari-Illiou, N. Brivois, S. Djediat, M.F. Benedetti and F. Fiévet, *Nano Lett.*, **6**, 866 (2006).
35. Z.B. Huang, X. Zheng, D.H. Yan, G.F. Yin, X.M. Liao, Y.Q. Kang, Y.D. Yao, D. Huang and B. Hao, *Langmuir*, **24**, 4140 (2008).